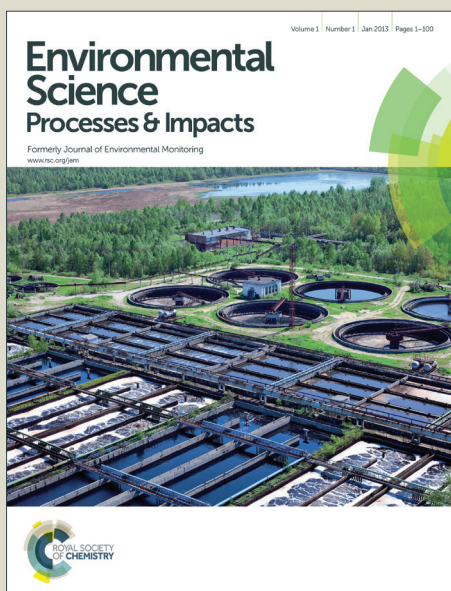


Environmental Science Processes & Impacts

Accepted Manuscript



This is an *Accepted Manuscript*, which has been through the Royal Society of Chemistry peer review process and has been accepted for publication.

Accepted Manuscripts are published online shortly after acceptance, before technical editing, formatting and proof reading. Using this free service, authors can make their results available to the community, in citable form, before we publish the edited article. We will replace this *Accepted Manuscript* with the edited and formatted *Advance Article* as soon as it is available.

You can find more information about *Accepted Manuscripts* in the [Information for Authors](#).

Please note that technical editing may introduce minor changes to the text and/or graphics, which may alter content. The journal's standard [Terms & Conditions](#) and the [Ethical guidelines](#) still apply. In no event shall the Royal Society of Chemistry be held responsible for any errors or omissions in this *Accepted Manuscript* or any consequences arising from the use of any information it contains.

Chromium(III) Oxidation by Biogenic Manganese Oxides of Varying Structural Ripening

Yuanzhi Tang^{1*}, Samuel M. Webb², Emily R Estes³, Colleen M Hansel^{3*}

¹School of Earth and Atmospheric Sciences, Georgia Institute of Technology, 311 Ferst Dr, Atlanta, GA 30332-0340

²Stanford Synchrotron Radiation Lightsource, Menlo Park, CA 94025

³Marine Chemistry and Geochemistry Department, Woods Hole Oceanographic Institution, Woods Hole, MA 02543

*Corresponding authors:

Yuanzhi Tang: Tel: 404-894-3814; E-mail: yuanzhi.tang@eas.gatech.edu

Colleen Hansel: Tel: 508-289-3738; Email: chansel@whoi.edu

Environmental Impact

Chromium (Cr) is a widespread anthropogenic contaminant that compromises ecosystem and human health. Transformation of the micronutrient and less mobile species Cr(III) to highly mobile and toxic Cr(VI) is strongly mediated by manganese (Mn) oxides. In fact, Mn oxides are the only oxidants of Cr(III) under most environmental conditions. Although Mn oxides are generally considered biogenic in origin, few studies have addressed the coupled role of reaction conditions and biogenic Mn oxide structure in Cr(III) oxidation. In this study we examined the effect of light, organic carbon content, pH, and structural ripening of biogenic manganese oxides on Cr(III) oxidation using Mn oxides produced by a marine bacterium within the widespread *Roseobacter* clade.

Abstract

Manganese (Mn) oxides, which are generally considered biogenic in origin within natural systems, are the only oxidants of Cr(III) under typical environmental conditions. Yet the influence of Mn biooxide mineral structural evolution on Cr(III) oxidation under varying geochemical conditions is unknown. In this study we examined the role of light, organic carbon, pH, and structure of biogenic Mn oxides on Cr(III) oxidation. Aging of Mn oxides produced by a marine bacterium within the widespread *Roseobacter* clade resulted in structural ripening from a colloidal hexagonal to particulate triclinic birnessite phase. The structurally diverse Mn oxides were then reacted with aqueous Cr(III) within artificial seawater in the presence or absence of carbon and light. Here we found that Cr(III) oxidation capacity was highest at near neutral pH and in the combined presence of carbon and light. Mn oxide ripening from a hexagonal to triclinic birnessite phase led to decreased Cr(III) oxidation in the presence of carbon and light,

whereas no change in reactivity was observed in the absence of carbon and/or in the dark. As only minimal Cr(III) oxidation was observed in the absence of Mn oxides, these results strongly point to coupled Mn oxide- and photo-induced generation of organic and/or oxygen radicals involved in Cr(III) oxidation. Based on Mn oxide concentration and structural trends, we postulate that Mn(II) produced from the oxidation of Cr(III) by the primary Mn oxide is recycled in the presence of organics and light conditions, (re)generating secondary hexagonal birnessite and thereby allowing for continuous oxidation of Cr(III). In the absence of this Mn oxide regeneration, Cr(III) induced structural ripening of the hexagonal birnessite precludes further Cr(III) oxidation. These results highlight the complexity of reactions involved in Mn oxide mediated Cr(III) oxidation and suggest that photochemical carbon reactions are requisite for sustained Cr(III) oxidation and persistence of reactive Mn oxides.

Key words: Bacteria, Roseobacter, Biogenic manganese oxides, Chromium, Oxidation, Organics, X-ray absorption spectroscopy (XAS, XANES, EXAFS)

1. Introduction

Chromium (Cr) is a significant anthropogenic metal contaminant in soils and aquatic systems due to its widespread industrial applications. The toxicity and transport behavior of Cr depend strongly on its valence state, with hexavalent and trivalent being the most common oxidation states. Cr(VI) compounds are typically soluble, mobile, bioaccessible, and are considered carcinogenic upon inhalation exposure. Cr(III) generally forms insoluble (oxyhydr)oxides and is an essential micronutrient^{1,2}.

In terrestrial and aquatic systems, a variety of compounds are capable of reducing Cr(VI) to Cr(III), such as organic matter, Fe(II), and reduced sulfur species^{1,3-5}. Following reduction, Cr(III) precipitates as pure Cr(III) or mixed Cr(III)-Fe(III) (oxy)hydroxide phases that have low solubility and typically lack long range structural order^{6,7}. However, within common environmental conditions, Mn(III, IV) (oxyhydr)oxides (hereafter referred to as Mn oxides) are capable of oxidizing Cr(III) to Cr(VI) and are, in fact, considered the only environmentally relevant Cr(III) oxidant^{5,8,9}. Given the widespread presence of Mn oxides within the environment, understanding reaction conditions and mechanisms of Mn oxide mediated Cr(III) oxidation is important for predicting Cr mobility and transport. Several previous studies have investigated the kinetics and mechanisms of Cr(III) oxidation by abiotic (synthetic or natural) Mn oxides, such as δ -MnO₂^{3,10-12}, birnessite¹¹⁻¹⁷, manganite¹⁸, todorokite¹⁵, pyrolusite⁵, and hydrous manganese oxide¹⁹. It has generally found that the rate and extent of Cr(III) oxidation was affected by the type and structure of Mn oxides^{15,20-22}. In particular, Mn oxides with hexagonal symmetry (biogenic Mn oxide and birnessite) have shown the highest oxidation capacity for Cr(III)²².

23 Natural Mn oxides are believed to form primarily by Mn(II) oxidation via either direct or
24 indirect microbial activity²³. The predominant type of biogenic Mn oxide formed at
25 circumneutral pH is a highly disordered, nanocrystalline, phyllomanganate phase, similar to
26 hexagonal birnessite²⁴⁻²⁶. This phase is highly reactive and can undergo abiotic transformation
27 and ripening to form more ordered and crystalline phases such as todorokite, feitknechtite, and
28 triclinic birnessite^{24, 27-29}. Due to their greater disorder and surface area, biogenic oxides are
29 considered more reactive than their synthetic analogs^{24, 25, 30}. Yet, only a few studies have
30 examined Cr(III) oxidation by Mn oxides produced by microorganisms, such as the Mn(II)-
31 oxidizing bacteria *Pseudomonas putida*^{22, 31-33} and *Bacillus* sp.^{22, 32}. These studies either used
32 the fresh biogenic Mn oxides (with a layered structure similar to δ -MnO₂) or characterized the
33 coupled Mn(II)-Cr(III) oxidation in the presence of active microbial Mn(II)-oxidizing activity.
34 To our knowledge, no previous studies have examined the impact of natural structural
35 transformations of biogenic Mn oxides on their reactivity toward Cr(III) oxidation.

36 Microorganisms (both bacteria and fungi) that are capable of oxidizing Mn(II) to
37 Mn(III,IV) oxides are widespread in both marine and terrestrial settings, as well as contaminated
38 sites^{23, 34, 35}. Recently, Mn(II) oxidation by some bacterial and fungal species has been linked to
39 the extracellular production of the reactive oxygen species (ROS) superoxide³⁴⁻³⁶. Oxidation by
40 a bacterium (*Roseobacter* sp. AzwK-3b) within the widespread and abundant *Roseobacter* clade
41 was attributed to an exoprotein (extracellular), such that superoxide production and Mn(II)
42 oxidation activity occurred outside the cell and thus activity was maintained in cell-free filtrate³⁶,
43³⁷. The initial oxidation of Mn(II) by these exoproteins within the cell-free filtrate results in the
44 formation of a highly reactive colloidal birnessite phase with hexagonal symmetry and similar in
45 structure to δ -MnO₂. This initial hexagonal birnessite phase is highly reactive and induces the

46 secondary abiotic oxidation of Mn(II). Mn(II)-induced aging of this colloidal phase introduces
47 structural reorganization and the gradual transformation to a particulate phase with trigonal
48 symmetry and minimal reactivity toward aqueous Mn(II)²⁷. Abiotic oxidation of Mn(II) at the
49 colloidal hexagonal birnessite surface was substantially enhanced in the presence of light and
50 organic carbon and diminished in the presence of superoxide scavengers (e.g., superoxide
51 dismutase – SOD), indicating a role for ROS and organic radicals in Mn(II) oxidation. Further, it
52 illustrates a tight coupling between microbial and mineral surface chemical processes responsible
53 for the oxidation of Mn(II). Given the structural evolution and subsequent changes in reactivity
54 of biogenic Mn oxides, this system provides an ideal opportunity for studying the structure-
55 reactivity relationship of biogenic Mn oxides in the oxidation of Cr(III).

56 Accordingly, in this study, we examined the oxidation of Cr(III) by Mn oxides produced
57 by biogenic extracellular superoxide over the course of mineral structural evolution. We further
58 explored the impact of pH, organic carbon content, and light on Cr(III) oxidation by these
59 structurally diverse biogenic oxides. Given the widespread presence of Mn(II) oxidizing
60 microorganisms in the environment, results from this study provide important insights regarding
61 the reactivity of biogenic Mn oxides, as well as the fundamental basis for predicting and
62 understanding Cr fate and transport behavior in nature.

63

64 **2. Materials and methods**

65 ***2.1. Bacterial growth and biogenic Mn Oxide harvesting process***

66 *Roseobacter* sp. AzwK-3b was grown in an organic carbon rich (K) medium containing 2
67 g/L peptone, 0.5 g/L yeast extract, and 20 mM HEPES buffer prepared with 75 vol.% artificial
68 seawater (ASW), pH 7.2 at 25 °C and 150 rpm³⁷ without MnCl₂. The ASW contains 0.3 mol/L

69 NaCl, 0.05 mol/L MgSO₄, 0.01 mol/L CaCl₂, and 0.01 mol/L KCl. After growing *R. AzwK-3b* to
70 mid exponential phase (OD₆₀₀ ~0.12), cell free filtrate was collected by centrifuging the growth
71 culture at 8,000 rpm for 10 min and passing the supernatant through a 0.45 μm filter. The
72 resulting solution is hereafter referred to as a cell free filtrate, which maintains the activity for
73 extracellular enzymatic superoxide production^{27, 36} and is used for producing biogenic Mn
74 oxides.

75 Biogenic Mn oxides (hereinafter referred to as bioMnOx) were produced by reacting the
76 cell free filtrate with 100 μM MnCl₂ at 25° C and 150 rpm in the presence of ambient light.
77 BioMnOx were aged and harvested at various time points (4–211 h) by centrifuging at 9,000 rpm
78 for 25 min and washing with deionized water (18 MΩ-cm).

79

80 **2.2. Cr(III) oxidation experiments**

81 Harvested bioMnOx were resuspended in 50 mL of sterile K medium or ASW at pH 6.2
82 or 7.2 (buffered by 20 mM HEPES) and tested for Cr(III)-oxidizing capacity in the presence or
83 absence of light. The initial bioMnOx concentration was ~40 μM, measured as Mn(III,IV) oxide
84 concentration using the Leucoberlelin blue (LBB) method (see details below)³⁸. Cr(III) was
85 added as CrCl₃ from a 100 mM sterile stock solution to achieve an initial concentration of 50 μM.
86 Flasks containing the suspension were shaken at 25 °C and 150 rpm for ~200 h in the absence
87 (dark condition) or presence of ambient light (light condition). For experiments conducted in
88 dark conditions, all solutions were prepared in bottles wrapped with aluminum foil, and the
89 reaction flasks further covered with a cardboard box. Sampling was done without direct light
90 exposure. Control experiments were conducted at the same Cr(III) concentration and reaction
91 conditions without the addition of bioMnOx. The effect of bioMnOx concentration on the Cr(III)

92 oxidation was also explored using up to 4 times concentrated bioMnOx (i.e., 1× to 4× of 40 μM
93 Mn(III,IV) oxide) and an initial Cr(III) concentration of 50 μM. All experiments were conducted
94 in duplicate.

95 During the course of reaction, Mn oxide loss and Cr(VI) production were constantly
96 monitored. Concentration of Mn(III, IV) oxides were quantified using the Leucoberlelin blue
97 (LBB) method with a UV-Vis spectrophotometer (Cary 50, Varian)³⁸. Standard curves were
98 obtained using LBB and synthetic δ-MnO₂²⁵. The concentration of Cr(VI) in the reacting
99 suspension was analyzed using the s-diphenyl carbazide method⁹. To account for unavoidable
100 minor variations in initial Mn oxide content, a Cr oxidation capacity is used to normalize the
101 amount of Cr(VI) production to the initial Mn(III, IV) oxide concentration, defined as:

$$102 \quad \text{Cr oxidation capacity} = [\text{Cr(VI)}] / [\text{Mn(III,IV) oxide}]_{\text{ini}},$$

103

104 **2.3. X-ray absorption spectroscopy analysis**

105 X-ray absorption spectroscopy (XAS) data were collected on the bioMnOx before and
106 after reaction with Cr(III) to identify speciation and structural changes. Suspensions containing
107 Mn oxides were vacuum filtered through 0.2 μm polycarbonate membranes and rinsed with DI
108 water. The moist filter membranes loaded with Mn oxide wet pastes were then mounted in a
109 Teflon sample holder covered with Kapton tape for XAS data analysis. Samples were frozen at -
110 20 °C and thawed prior to analysis. Manganese K-edge XAS spectra were collected at beamline
111 11-2 at Stanford Synchrotron Radiation Lightsource (SSRL) and beamline X18B at National
112 Synchrotron Light Source, Brookhaven National Laboratory (NSLS-BNL) with a Si (220) or
113 (111) double crystal monochromator (40% detuning), respectively. Energy calibration was
114 achieved using a Mn foil (6539 eV). Data were collected in both fluorescence and transmission

115 mode using a 30-element Ge solid-state detector with a Cr filter at beam line 11-2 (SSRL) or a
116 PIPS detector at beam line X18B (NSLS). Analysis of the near edge region of consecutive XAS
117 spectra for each sample showed no photo-induced reduction of Mn oxides under the X-ray beam.

118 Analysis of the bulk XAS data was performed using the programs SIXPACK³⁹ and Ifeffit
119⁴⁰. The composition and structure of Mn oxides were determined using both the XANES (X-ray
120 absorption near edge structure) and EXAFS (extended X-ray absorption fine structure) regions.
121 For EXAFS analysis, spectra were background-subtracted, k^3 -weighted and analyzed from 3–12
122 Å⁻¹. As previously described^{24,27}, principal component analysis (PCA), combined with target
123 transformation and linear combination fitting (LCF), were performed on the EXAFS spectra to
124 establish the number of components representing the entire data set. A spectral reference library
125 of model Mn compounds was used to identify and quantify the structural components. The
126 model compounds used were previously described²⁴, and include: δ -MnO₂, triclinic Na-
127 birnessite, hexagonal Ca-birnessite, groutite (α -MnOOH), feitknechtite (β -MnOOH), manganite
128 (γ -MnOOH), hausmannite (Mn₃O₄), synthetic todorokite [(Na,Ca,K)(Mg,Mn)Mn₆O₁₄·5H₂O],
129 pyrolusite (β -MnO₂), synthetic Mn₂O₃, aqueous Mn(III) pyrophosphate, aqueous MnCl₂, and
130 aqueous MnSO₄.

131 To determine the detailed structure of the nanoparticulate and highly disordered
132 manganese oxides, a full multiple scattering model²⁶ that is sensitive to the bending of the Mn
133 octahedral layer and Mn site vacancies was used to conduct shell-by-shell EXAFS fitting. This
134 model has been previously described in detail^{26,27} and is briefly summarized below. The model
135 consists of all single scattering (SS) paths and three types of collinear multiple scattering (MS)
136 paths. The amplitude of all MS paths is strongly affected by the level of distortion of the
137 phyllomanganate layers, which is accounted for as an out-of-plane bending angle β (along the a -

138 axis)^{26, 41}. A parameter f_{occ} characterizes the lattice occupancy and accounts for both the
139 vacancies within the phyllosmanganate layer as well as edge effects in nanoparticulate Mn oxides.
140 .

141 **3. Results and Discussions**

142 **3.1. Production of structurally evolved Mn oxides**

143 Similar to previous observations²⁴⁻²⁶, the predominant form of biogenic Mn oxides
144 formed at circumneutral pH was a highly disordered layered phyllosmanganate phase with
145 hexagonal symmetry. Principle component analysis (PCA) using a suite of Mn reference
146 compounds indicated that two components were needed to reconstruct all of the unreacted
147 bioMnOx Mn EXAFS spectra, and these components were identified as a hexagonal birnessite
148 phase (δ -MnO₂) and a triclinic birnessite phase (Na-birnessite) (Figure 1a). The difference
149 between these two structures are most distinctive at around 7–10 Å⁻¹ in k space (gray shading in
150 Figure 1a). The hexagonal phase shows two distinct peaks at ~8 and 9 Å⁻¹, whereas for the
151 triclinic phase the 8 Å⁻¹ oscillation decreases in amplitude accompanied with a broadening of the
152 feature at ~9 Å⁻¹. Linear combination fitting (LCF) using the two reference compounds yielded
153 good fits for all bioMnOx samples (Table S1 and Figure 1b dotted line). The structure of the
154 fresh (4 h) bioMnOx was composed of 100% hexagonal birnessite, and appeared as brownish
155 suspended colloids. Upon aging, a triclinic birnessite structure was needed to fit the bioMnOx
156 spectra. With increased aging time, the fraction of the triclinic birnessite phase increased, and the
157 bioMnOx also aggregated to larger dark brown to black particles. At 211 h, the bioMnOx
158 structure was best fit with 56% hexagonal and 44% triclinic birnessite. A near linear relationship
159 ($R^2 = 0.9238$) between the fraction of hexagonal birnessite phase and aging time was observed
160 (Figure 1b), suggesting a strong correlation between bioMnOx structure and aging time.

161 These results are consistent with previous experiments using the same organism and
162 similar experimental conditions²⁷. In detail, Learman et al²⁷ reported the transformation of
163 bioMnOx from a pure hexagonal birnessite phase at 4 h to a 45% hexagonal/55% triclinic phase
164 at 96 h. Similarly, using synchrotron X-ray diffraction and absorption spectroscopy, Webb et al
165²⁶ found that the initial bioMnOx produced by the spores of a marine *Bacillus sp.* was a layered
166 phyllomanganate with hexagonal sheet symmetry similar to that of δ -MnO₂ and transformed to
167 pseudo-orthogonal sheet symmetry with a structure similar to that of triclinic birnessite. These
168 results are in agreement with our findings and suggest that a gradual structural transformation of
169 bioMnOx can be common in the nature, and might play an important role in the bioMnOx
170 reactivity toward controlling metal speciation such as the oxidation of Cr(III).

171 Detailed structural fitting of the initial Mn oxides were consistent with the LCF results
172 (Figure 2, Table S2). In particular, the initial colloidal Mn oxide phase (4 h) had a structure with
173 a negligible out-of-plane bending of the octahedral layers ($\beta_a = 0$), a high number of corner-
174 sharing Mn octahera (CN = 3.2), and low fraction of occupied Mn octahedral sites ($f_{occ} = 0.64$).
175 These values are in good agreement with the structural model for hexagonal birnessite²⁶ with a
176 slightly lower f_{occ} value. Upon aging, the bioMnOx gradually transformed with structural
177 parameters intermediate between hexagonal and triclinic birnessite. The out-of-plane bending
178 angle β_a increased from zero to ~1.6, 6.9, and 7.4 for bioMnOx aged for 31, 96 and 211 hours,
179 respectively, suggesting a gradual transformation of the bioMnOx from hexagonal to triclinic
180 symmetry over time and is consistent with the LCF results. Triclinic birnessite has pseudo-
181 orthogonal symmetry and is characterized by a larger proportion (up to 1/3) of Mn(III) octahedra
182 in the sheets compared to hexagonal birnessite^{42, 43}. The large angular non-linearity along a -axis

183 (β_a 12–17)^{26, 41} of triclinic birnessite is a result of lattice strain produced in the planar sheet
184 buckling upon Mn(III)-rich row formation⁴².

185 Further and as expected, the dominant oxidation state of the bioMnOx was Mn(IV) with a
186 minor component of Mn(III). Comparing the peak crest positions of bioMnOx with those of the
187 reference compounds (vertical dotted lines), indicated that the bioMnOx all have a Mn valence
188 state similar to that of δ -MnO₂, which has an average oxidation state of 3.9–4.0 (Figure S1).
189 However, all bioMnOx spectra also showed peak broadening, with a small shoulder at ~6550 eV
190 that is similar to that of the feitknechtite spectra, suggesting the presence of minor amounts of
191 Mn(III) in the structure.

192

193 ***3.2. Cr(III) oxidation by structurally diverse biogenic Mn oxides under varying light and*** 194 ***carbon conditions***

195 The extent of Cr(VI) production was 2–10 times higher in the presence relative to
196 absence of bioMnOx, indicating that the biogenic Mn oxides induced the oxidation of aqueous
197 Cr(III) (Figure 3). In detail, Cr(VI) production in the absence of Mn oxides averaged 0.55 μ M,
198 (1.1% of added Cr(III)) which was substantially lower than that in the presence of bioMnOx
199 (Figure 3). Interestingly, control experiments conducted in the absence of Mn oxides and within
200 the dark yielded Cr(VI) production close to zero, whereas those in the light within either cell-free
201 filtrate, ASW, or K medium yielded small amounts of Cr(VI) production (0.5–1.5 μ M). These
202 values, although far less than those in the presence of bioMnOx, suggest a potential contribution
203 of photo-active factors, such as reactive oxygen species (ROS) or organic radicals produced in
204 the presence of light, in oxidizing Cr(III).

205 In the presence of bioMnOx, the rate and extent of Cr(III) oxidation varied as a function
206 of Mn oxide structure (age), light, and organic carbon. In the absence of organic carbon (i.e., in
207 ASW) and/or under dark conditions, a significant difference between the Cr(III) oxidation
208 capacity of differently aged MnOx was not observed (Figure 4). However, in organic carbon-rich
209 K medium in the presence of light, the Cr(III) oxidation capacity is highly dependent on MnOx
210 structure (age). In particular, more aged bioMnOx phases with a higher proportion of triclinic
211 birnessite demonstrated lower reactivity. In fact, a linear correlation ($R^2 = 0.9897$; dotted line in
212 Figure 4) between Cr(III) oxidation capacity and MnOx age can be established. Note that all
213 experiments were conducted with the same concentration of initial MnOx and Cr(III), therefore
214 the differences in reactivity was likely due to variation in the intrinsic reactivity as the oxides
215 aged from hexagonal to triclinic birnessite.

216 Despite many previous studies, the detailed reaction mechanism(s) of Cr(III) oxidation by
217 Mn oxides remain unclear. It was showed that the Cr(III) oxidation ability of different
218 manganese oxides can be related to, although not directly proportional to, the presence of
219 structural Mn(III)²¹. The availability of Mn(III) during the oxidation of Cr(III) by δ -MnO₂ was
220 also shown to be an important controlling factor in that the presence of Mn(III) complexing
221 ligand pyrophosphate during the reaction between Cr(III) and Mn oxide drastically reduced
222 Cr(III) oxidation rate¹³. The presence of Mn(II) has also been shown to enhance Cr(III)
223 oxidation by synthetic manganese oxides (e.g., hausmannite, Mn₃O₄)²¹ or in systems containing
224 Mn(II)-oxidizing microorganisms^{22, 31-33}. For these biotic systems, it is generally recognized that
225 the oxidation of Cr(III) is mainly due to the formation of biogenic Mn oxides that are produced
226 from the oxidation of Mn(II) by microorganisms^{23, 34-36}. However, in these studies, the presence
227 of active cells complicates the investigations due to cell metabolism and/or the toxicity effect of

228 Cr(VI), thus making it difficult to isolate the structural effect of the biologically formed Mn
229 oxides. Here, we show too that light and organic carbon (Figure 3–5, Table 1) complicates the
230 direct assessment of the role of Mn oxide structure and composition on Cr(III) oxidation.

231 In particular, a substantial structural influence in the presence of carbon and light was
232 observed for the initial hexagonal birnessite dominated Mn oxide phases (aged less than 50
233 hours). For 4 h old Mn oxides, the Cr(III) oxidation capacity was highest under combined light
234 and carbon conditions, reaching ~ 0.20 at near steady state; whereas all other conditions (K dark,
235 ASW light, or ASW dark) showed similar Cr(III) oxidation capacity of ~ 0.07 (Figure 5 a). As
236 minimal Cr(VI) was produced in K light condition in the absence of Mn oxides, a mineral
237 surface produced photoactive factor was likely at play. Mn oxides are versatile oxidants of a
238 wide range of organic compounds such as hydroquinone, oxalic acid, and humic substances⁴⁴⁻⁴⁷,
239 and the Mn oxide catalyzed oxidation of organics are known to produce reactive organic radicals
240^{45, 48}. Similarly, Learman et al²⁷ implicated both mineral induced organic and oxygen radical
241 formation in accelerated Mn(II) oxidation rates by colloidal hexagonal birnessite formed by this
242 *Roseobacter* species. On the other hand, it is worth noting that Cr(III) can strongly complex with
243 organic ligands such as citrate and EDTA, which can prevent the release of Cr(III) ions and
244 subsequent oxidation by Mn oxides^{14, 17}. Although we observed enhanced Cr(VI) formation in
245 the presence of organics, complexation of Cr(III) by media components (K medium is a rich
246 medium containing peptone and yeast extract) could hypothetically limit the extent of Cr(VI)
247 formation. At this stage, the exact photo-active factor or organic compound(s) in our system is
248 not clearly understood; partially due to the fact the K medium is a rich organic matrix composed
249 of a large diversity of organic nitrogen and carbon molecules. The identity of the reactive
250 organic(s) and the reaction mechanisms are currently under investigation.

251 Interestingly, despite differences in Cr(VI) production by the initial hexagonal birnessite
252 phase incubated under different conditions (Figure 5a), a concomitant change in Mn oxide
253 concentration was not observed (Figure 5b). In detail, all experiments showed a similar sharp
254 decrease in the Mn oxide concentration to ~65% of the initial concentration within 20 h,
255 followed by a pseudo steady state level that was maintained at ~60% throughout the remainder
256 of the reaction (Figure 5b). The 4 and 31 h aged bioMnOx showed similar Cr(VI) production and
257 MnOx consumption trends (Figure 5a-d). For the more triclinic bioMnOx (211 h aged), however,
258 differences in Cr(VI) production and MnOx consumption varied based on the experimental
259 conditions, with the carbon replete (K) light incubations still yielding the highest Cr(VI)
260 production and the carbon-deplete (ASW) dark condition showed the largest loss of Mn(III,IV)
261 oxide.

262 The change in Mn oxide concentration likely involved a number of reactions, including
263 decreased MnOx concentration through the redox reaction with Cr(III), photo-induced
264 dissolution, and increased MnOx concentration via the abiotic oxidation of aqueous Mn(II) at the
265 Mn oxide surface (production of secondary Mn oxides)⁴⁹. Mn oxides^{50,51}, especially highly
266 reactive layered phyllosulfates⁵², can accelerate the oxidation of Mn(II) by O₂ through
267 autocatalysis. Further, Learman et al²⁷ reported hexagonal birnessite- and light-mediated
268 formation of carbon and oxygen radicals can lead to Mn(II) oxidation rates in excess of the
269 competing photodissolution process²⁷. Based on our Mn oxide and Cr(VI) concentration data,
270 we postulate that this Mn (re)cycling is a likely mechanism responsible for the high Cr(III)
271 oxidation capacity in the combined presence of light and organics in our system. In detail, during
272 the initial 20 h, during which Mn(III, IV) oxide concentration experienced a sharp decrease, the
273 system is dominated by the redox reaction between primary bioMnOx and Cr(III), which

274 produces Cr(VI) and presumably aqueous Mn(II). The produced Mn(II) can then be oxidized by
275 carbon and/or oxygen radicals produced by reaction with the remaining bioMnOx to produce
276 more secondary MnOx, which are also capable of oxidizing Cr(III). This process (cycling of
277 Mn(II)) might explain the apparent higher Cr(III) oxidation capacity yet near steady state
278 concentration of Mn oxide in the system. Alternatively, the carbon- and/or oxygen-radicals could
279 directly oxidize Cr(III) – yet, this would not explain the Mn oxide concentration trends (Figure
280 5b) in combination with the persistence of hexagonal birnessite in the presence of light and
281 carbon (discussed below).

282

283 ***3.3. Rates of Cr(III) Oxidation***

284 For all conditions, the rates of Cr(III) oxidation were fastest during the initial 20 h,
285 slowly decreasing over time and plateauing between 50 and 150 hours (e.g., Figure 5a, c, and e).
286 Initial Cr(III) oxidation rates, based on the amount of Cr(VI) production during the first 20 h,
287 spanned an order of magnitude and were highly dependent upon the structure of the Mn oxide
288 and the aqueous conditions (Table 1). For instance, the initial Cr(III) oxidation rate for the 4 h
289 old bioMnOx was 0.11–0.29 $\mu\text{M h}^{-1}$ under K light condition, 0.02–0.03 $\mu\text{M h}^{-1}$ at K dark
290 condition, and 0.02–0.11 $\mu\text{M h}^{-1}$ at ASW conditions (light and dark).

291 Previous studies on the oxidation of Cr(III) by various manganese oxides showed varied
292 reaction rates and capacity. Using Q-XAFS (quick X-ray absorption fine structure spectroscopy),
293 Landort et al ¹¹ showed that the oxidation of Cr(III) by three different types of synthetic poorly
294 crystalline layered manganese oxides ($\delta\text{-MnO}_2$, random stacked birnessite, and acid birnessite)
295 were fast within the first 30 min and ceased between 30 min and 1 h, which was explained as the
296 sorption of Cr(VI) species on the Mn oxides. Dai et al ¹⁷ also observed a fast increase of Cr(VI)

297 levels in the presence of δ -MnO₂ within the initial ~50 min, followed by very slow increase of
298 Cr(VI) after 300 min, which was explained as the saturation of available surface adsorption sites.

299 Due to the difference in experimental conditions, it is difficult to directly compare the
300 oxidation rates from our system with previous studies. Therefore we compared our results with
301 Mn(II) oxidation rates by these same biooxides²⁷. Consistent with Cr(III) oxidation, Learman et
302 al²⁷ found that more aged (more triclinic) bioMnOx phases yielded lower Mn(II) oxidation.
303 Using 4 h aged colloidal hexagonal birnessite, they reported Mn(II) oxidation rates of 0.56–2.30
304 $\mu\text{M h}^{-1}$ in the presence of organic carbon (K media) and light, 0.21–0.62 $\mu\text{M h}^{-1}$ in K within the
305 dark, and 0.08–0.27 $\mu\text{M h}^{-1}$ in the absence of organic carbon (ASW). These values are
306 substantially higher than the Cr(III) oxidation rates observed here, likely due to the difference in
307 the nature of the reaction mechanism(s), e.g., 3 electrons are needed to oxidize Cr(III) to Cr(VI),
308 whereas only 1–2 electrons are needed to oxidize Mn(II) to Mn(III) or Mn(IV). However, both
309 datasets follow a general trend that the combination of light and organic carbon yielded higher
310 oxidation rates.

311

312 ***3.4. Mn oxide structural changes upon reaction with Cr(III)***

313 The reacted bioMnOx samples appeared to be more triclinic as compared to the reference
314 compound δ -MnO₂ (hexagonal birnessite structure), with a diminished oscillation at $\sim 8 \text{ \AA}^{-1}$ and
315 broad feature at $\sim 9 \text{ \AA}^{-1}$ (Figure 2). Detailed structural analysis revealed that all reacted samples
316 transformed from the highly disordered hexagonal birnessite phase into more ordered phases
317 similar to triclinic birnessite (Figure 6 and Table S2). For instance, the out-of-plane bending
318 angles β_a are generally much higher than those of the unreacted samples. Interestingly, the 4 h
319 aged bioMnOx, which possessed the highest oxidative capacity for Cr(III) in the presence of

320 light and organic carbon (Figure 4) yielded final Mn oxides with a lower β_a angle than the other
321 three conditions (K dark, ASW light, and ASW dark) (Figure 6). The 31 h aged bioMnOx also
322 showed a lower β_a angle in K light condition compared to the ASW dark condition. These
323 observations are consistent with our hypothesis that Mn(II) produced from the redox reaction
324 between Cr(III) and the (primary) bioMnOx was recycled in the system and induced the
325 (re)precipitation of (secondary) hexagonal birnessite. Such cycling was dominant in carbon-
326 replete light conditions and the produced secondary Mn oxides restored the hexagonal Mn oxide
327 reservoir in the system, thus resulting in an apparent steady state of MnOx concentration (Figure
328 5b and d) as well as lower β_a angles that correspond with the presence of more hexagonal phases
329 (Figure 6).

330 In contrast, the 211 h aged bioMnOx had similar β_a angles after reaction under carbon-
331 replete (K) light and -deplete (ASW) dark conditions. This is consistent with a similar lack in
332 Cr(VI) production under these conditions (Figure 4) and is likely due to the low reactivity of
333 these more aged bioMnOx toward Cr(III) oxidation, Mn(II) oxidation, and thus production of
334 secondary MnOx. The fact that both β_a angles were lower than those of the 4 and 31 h aged
335 bioMnOx under dark and carbon-deplete (ASW) conditions is consistent with the overall low
336 reactivity of 211 h aged bioMnOx.

337

338 **3.5. Effect of pH and Mn oxide concentration**

339 Cr(III) oxidation by abiotic Mn oxides has a strong pH dependence^{3, 15}. Here the
340 oxidation of Cr(III) by 96 h aged bioMnOx reacted in the organic rich medium (K) under light
341 conditions was substantially greater at pH 7.2 relative to 6.2 (Figure 7b). At pH 7.2, Cr(III)
342 oxidation had a fast initial reaction (within ~40 h) followed by a slow yet continuous process that

343 reached steady state only after ~150 h, resulting in a final Cr oxidation capacity of ~0.16 (Figure
344 7b). Correspondingly, the amount of bioMnOx in the reacting suspension quickly dropped to
345 87% within ~40 h, and slowly continued to ~80% after 160 h (Figure 7a). The increase in Cr(VI)
346 and decrease of bioMnOx levels was presumably dominated by the redox reaction between
347 Cr(III) and bioMnOx, which involved the oxidation of Cr(III) to Cr(VI) and the reduction of
348 Mn(III, IV) oxides to soluble Mn(II) species.

349 Interestingly, at pH 6.2 the Cr(III) oxidation capacity quickly increased to ~0.06 within
350 ~10 h at a rate similar to that at pH 7.2, but then remained at this level throughout 160 h of
351 reaction with no further significant production of Cr(VI) (Figure 7b). Mn oxide concentration
352 decreased to ~85% during the first 10 h, and drastically dropped to only ~25% after 160 h
353 reaction time (Figure 7a). These observations are strikingly different from that at pH 7.2. At low
354 pH, less Cr(VI) was produced but there was much greater loss of Mn(III, IV) oxides. In contrast,
355 higher pH resulted in a much higher and continuous production of Cr(VI), accompanied by a
356 near steady-state concentration of Mn oxides.

357 Several studies have examined the effect of pH on Cr(III) oxidation by synthetic Mn
358 oxides^{3, 10, 15}, with an emphasis at acidic pH ranges. These studies observed that Mn oxides can
359 strongly oxidize Cr(III) at lower pH ranges, and the pH effects were mainly contributed to two
360 processes: (1) the adsorption of Cr(III) species on the surface of Mn oxides, which increases with
361 increasing pH due to increased surface negative charge, and is favorable for more Cr(III)
362 oxidation; and (2) the complexation of Cr(III) with hydroxyl groups and potential precipitation
363 of Cr(III)-(oxyhydr)oxide phases, which is enhanced with increasing Cr(III) concentration and
364 pH, and significantly decreases Cr(III) oxidation by Mn oxides. In our system, with the low
365 Cr(III) concentration employed (50 μ M), we do not expect the second mechanism to be

366 significant. In fact, speciation calculations using the program Phreeqc⁵³ indicated that at both pH
367 values our system was undersaturated with respect to solid Cr(III) (oxyhydr)oxide phases and the
368 dominant Cr(III) species were $\text{Cr}(\text{OH})_2^+$ and CrOH^{2+} .

369 The observations in our system appeared to be contradictory to previous studies in that a
370 higher pH value yielded higher Cr(III) oxidation in our system. However, it is worth noting that
371 all those studies used synthetic Mn oxides. In a few studies examining the oxidation of Cr(III) by
372 biogenic manganese oxides formed *in situ*, pH were controlled at near circumneutral values to
373 maintain cell activity^{22, 31-33}. It is possible that (1) the biogenic Mn oxides formed under these
374 conditions (including our system) might undergo proton-promoted dissolution at reduced pH
375 conditions; and/or (2) that the activity of these biogenic Mn oxides toward Mn(II) oxidation and
376 production of secondary Mn oxides is lower at low pH values. The detailed reaction
377 mechanism(s) as well as the changed reactivity of bioMnOx under low pH conditions are under
378 active investigation.

379 The Cr(III) oxidation capacity was also dependent on the initial bioMnOx concentration.
380 Under both carbon-rich (K) light and -deplete (ASW) dark conditions, higher initial bioMnOx
381 concentrations resulted in decreased Cr(III) oxidation capacity (Figure S2). Consistent with our
382 previous observations, Cr(VI) oxidation efficiencies were higher under K light than ASW dark
383 condition. All values were obtained after the reaction proceeded for ~150 h, representing near
384 steady state values. Given all the same reaction conditions, one might expect the Cr(III)
385 oxidation capacity to maintain a constant value regardless of Mn oxide concentration. The fact
386 that it decreased with increasing Mn oxide concentration was likely due to aggregation effects.
387 Mineral particle aggregation and/or collision at high concentrations can decrease the effective
388 surface area and result in lower degrees of contact with Cr(III).

389

390 **4. Environmental Implications**

391 To our knowledge, this is the first study exploring the effect of structural evolution of
392 biogenic Mn oxides on the oxidation of Cr(III) under various geochemical conditions. Here, as
393 schematically illustrated in Figure 8, we show that Cr(III) oxidation occurs to a much greater
394 extent via reaction with hexagonal birnessite in the presence of both light and organic carbon.
395 The production of photo-active factors, presumably organic- and/or oxygen- radicals, likely
396 induce the (re)cycling of Mn in the system yielding substantially higher Cr(III) oxidation extent
397 and rates. These surface mediated reactions in the presence of light and organics is apparently
398 great enough to offset photo-dissolution of Mn oxides and allow for sustained oxidative capacity.
399 The regeneration of reactive hexagonal birnessite under these conditions suggests that the
400 speciation and fate of Cr in the natural environment might be dictated by even just a small
401 amount of Mn oxides. Given the ubiquitous presence of Mn oxides in nature and that
402 nanoparticulate hexagonal birnessite is the dominant Mn oxide formed by both terrestrial and
403 marine microorganisms, this cycling scenario might play a substantial role in controlling the
404 speciation of numerous redox sensitive elements, such as other metals and organic compounds.

Acknowledgements

The authors acknowledge funding support by Georgia Institute of Technology to YT and NSF grant CBET-1336496 to CMH. Portions of this research were conducted at the Stanford Synchrotron Radiation Lightsource (SSRL) and the National Synchrotron Light Source (NSLS). SSRL is a Directorate of SLAC National Accelerator Laboratory and an Office of Science User Facility operated for the U.S. Department of Energy Office of Science by Stanford University. NSLS is supported by the US Department of Energy, Office of Science, Office of Basic Energy Sciences, under Contract No. DE-AC02-98CH10886. Comments from two anonymous reviewers helped improving the manuscript.

Electronic Supplementary Information Available

XANES of reference compounds, unreacted, and reacted Mn oxides; Mn K-edge EXAFS fitting results of reference compounds and bioMnOx before and after reaction with Cr(III); Cr oxidation capacity as a function of bioMnOx concentration. This information is available at DOI:xxx.

Figure Captions

Figure 1. (a) Linear combination fitting (LCF) results of unreacted bioMnOx at different ages, with raw and fitted data in solid and dotted black lines, respectively. Also shown are the two end member spectra (gray lines) used for LCF, a hexagonal birnessite (δ -MnO₂) and triclinic Na-birnessite. (b) Corresponding LCF fraction of hexagonal and triclinic birnessite for the bioMnOx. Dotted line is a linear fitting of the hexagonal data ($R^2 = 0.9238$).

Figure 2. Mn K-edge EXAFS data (a) and corresponding Fourier transforms (b) of reference compounds (grey lines) and bioMnOx before (blue lines) or after (black lines) reacting with Cr(III) (~200 h). Raw and fitted data are shown in solid and dashed lines, respectively. Square with dotted line in (a) shows the “indicator” region of Mn EXAFS. Vertical dotted line in (b) labels the peak with major contributions from multiple scattering.

Figure 3. Amount of Cr(VI) produced in the presence of 4 h aged bioMnOx (filled bars) in artificial sea water (ASW) or K medium (K) at pH 7.2 under light (L) or dark (D) conditions. Also shown are the Cr(VI) production in control experiments (open bars), with the same amount of initial Cr(III) and no bioMnOx addition. They are conducted either in the cell-free filtrate, ASW, or K medium under light or dark conditions. Vertical dotted line is the averaged Cr(VI) production from all control experiments (0.55 μ M). All values were measured when reactions reached near steady state (~200 h).

Figure 4. Cr oxidation capacity as a function of bioMnOx age when reacted in K medium or ASW under light or dark conditions. Dotted line is a linear fitting of the K light data ($R^2 = 0.9897$). Reactions were conducted at pH 7.2.

Figure 5. Cr(III) oxidation capacity (a, c, e) and percent change of Mn(III, IV) oxide concentration (b, d, f) as a function of reaction time in the K medium or ASW under light or dark conditions. BioMnOx ages are 4 h (a and b), 31 h (d and e), and 211 h (e and f)

Figure 6. Comparison of the out-of-plane bending along a -axis (β_a angle) derived from EXAFS fitting of bioMnOx with different age and structural ripening before and after reaction with Cr(III) under different conditions.

Figure 7. Percent change of Mn(III,IV) oxide concentration (a) and Cr(III) oxidation capacity (b) as a function of reaction time at pH 6.2 and 7.2. Reaction condition: 96 h aged bioMnOx, K medium, light condition.

Figure 8. Schematic of possible reaction mechanism. Orange arrows represent reactions that occur only in the combined presence of organics and light.

Table 1. Initial Cr(III) oxidation rate and total Cr(VI) production. All reactions conducted at pH 7.2 in either K medium or ASW under light or dark conditions.

Reaction condition	BioMnOx age (h)	n ^a	Initial Cr(III) oxidation rate ^b ($\mu\text{mol L}^{-1} \text{h}^{-1}$)	Total Cr(VI) production ^c (μM)
K light	4.5	6	0.11 - 0.29	9.92 ± 3.11
	12	2	0.29 - 0.34	10.42 ± 0.36
	31	1	0.2	11.20
	96	3	0.15	6.15 ± 0.05
	211	2	0.09	1.97 ± 0.32
K dark	4.5	3	0.02 - 0.03	3.53 ± 1.30
	31	1	0.06	4.36
	211	2	0.02	1.45 ± 0.08
ASW light	4.5	5	0.03 - 0.09	3.76 ± 0.75
	12	2	0.15	4.46 ± 0.05
	24	3	0.08 - 0.09	3.23 ± 0.12
	31	1	0.09	2.72
	96	3	0.13 - 0.16	4.56 ± 0.18
	211	2	0.06	2.29 ± 0.12
ASW dark	4.5	4	0.02 - 0.11	3.70 ± 1.24
	31	1	0.08	2.66
	211	2	0.05	3.04

^a Total number of experiments conducted at this condition;

^b The rate of Cr(VI) production within initial 20 h;

^c The total amount of Cr(VI) produced in the reaction systems at near steady state (~200 h).

References

1. C. D. Palmer and P. R. Wittbrodt, *Environ. Health Perspect.*, 1991, **92**, 25-40.
2. R. P. Beliles, in *Toxicity of Heavy Metals in the Environment (Part II)*, ed. F. W. Oehme, M. Dekker, New York, 1979.
3. S. E. Fendorf and R. J. Zasoski, *Environ. Sci. Technol.*, 1992, **26**, 79-85.
4. Y. Z. Tang and S. T. Martin, *Geochim. Cosmochim. Acta*, 2011, **75**, 4951-4962.
5. L. E. Eary and D. Rai, *Environ. Sci. Technol.*, 1987, **21**, 1187-1193.
6. Y. Z. Tang, F. M. Michel, L. H. Zhang, R. Harrington, J. B. Parise and R. J. Reeder, *Chem. Mater.*, 2010, **22**, 3589-3598.
7. B. M. Sass and D. Rai, *Inorg. Chem.*, 1987, **26**, 2228-2232.
8. S. E. Fendorf, *Geoderma*, 1995, **67**, 55-71.
9. R. Bartlett and B. James, *Journal of Environmental Quality*, 1979, **8**, 31-35.
10. S. E. Fendorf, M. Fendorf, D. L. Sparks and R. Gronsky, *J. Colloid Interface Sci.*, 1992, **153**, 37-54.
11. G. Landrot, M. Ginder-Vogel, K. Livi, J. P. Fitts and D. L. Sparks, *Environ. Sci. Technol.*, 2012, **46**, 11594-11600.
12. G. Landrot, M. Ginder-Vogel, K. Livi, J. P. Fitts and D. L. Sparks, *Environ. Sci. Technol.*, 2012, **46**, 11601-11609.
13. P. S. Nico and R. J. Zasoski, *Environ. Sci. Technol.*, 2000, **34**, 3363-3367.
14. Y. M. Tzou, R. H. Loeppert and M. K. Wang, *Soil Science*, 2002, **167**, 729-738.
15. X. H. Feng, L. M. Zhai, W. F. Tan, W. Zhao, F. Liu and J. Z. He, *J. Colloid Interface Sci.*, 2006, **298**, 258-266.
16. C. Oze, D. K. Bird and S. Fendorf, *Proceedings of the National Academy of Sciences of the United States of America*, 2007, **104**, 6544-6549.
17. R. A. Dai, J. Liu, C. Y. Yu, R. Sun, Y. Q. Lan and J. D. Mao, *Chemosphere*, 2009, **76**, 536-541.
18. R. M. Weaver, M. F. Hochella and E. S. Ilton, *Geochim. Cosmochim. Acta*, 2002, **66**, 4119-4132.
19. G. Landrot, M. Ginder-Vogel and D. L. Sparks, *Environ. Sci. Technol.*, 2010, **44**, 143-149.
20. J. G. Kim, J. B. Dixon, C. C. Chusuei and Y. J. Deng, *Soil Sci. Soc. Am. J.*, 2002, **66**, 306-315.
21. R. M. Weaver and M. F. Hochella, *Am. Mineral.*, 2003, **88**, 2016-2027.
22. J. Z. He, Y. T. Meng, Y. M. Zheng and L. M. Zhang, *J. Soils Sed.*, 2010, **10**, 767-773.
23. B. M. Tebo, J. R. Bargar, B. G. Clement, G. J. Dick, K. J. Murray, D. Parker, R. Verity and S. M. Webb, *Annual Review of Earth and Planetary Sciences*, 2004, **32**, 287-328.
24. J. R. Bargar, B. M. Tebo, U. Bergmann, S. M. Webb, P. Glatzel, V. Q. Chiu and M. Villalobos, *Am. Mineral.*, 2005, **90**, 143-154.
25. M. Villalobos, B. Toner, J. Bargar and G. Sposito, *Geochim. Cosmochim. Acta*, 2003, **67**, 2649-2662.
26. S. M. Webb, B. M. Tebo and J. R. Bargar, *Am. Mineral.*, 2005, **90**, 1342-1357.
27. D. R. Learman, S. D. Wankel, S. M. Webb, N. Martinez, A. S. Madden and C. M. Hansel, *Geochim. Cosmochim. Acta*, 2011, **75**, 6048-6063.
28. X. H. Feng, M. Q. Zhu, M. Ginder-Vogel, C. Y. Ni, S. J. Parikh and D. L. Sparks, *Geochim. Cosmochim. Acta*, 2010, **74**, 3232-3245.

29. E. J. Elzinga, *Environ. Sci. Technol.*, 2011, **45**, 6366-6372.
30. B. M. Tebo, H. A. Johnson, J. K. McCarthy and A. S. Templeton, *Trends Microbiol.*, 2005, **13**, 421-428.
31. Y. X. Wu, B. L. Deng, H. F. Xu and H. Kornishi, *Geomicrobiol. J.*, 2005, **22**, 161-170.
32. K. J. Murray and B. M. Tebo, *Environ. Sci. Technol.*, 2007, **41**, 528-533.
33. K. J. Murray, M. L. Mozafarzadeh and B. M. Tebo, *Geomicrobiol. J.*, 2005, **22**, 151-159.
34. C. M. Hansel, C. A. Zeiner, C. M. Santelli and S. M. Webb, *Proceedings of the National Academy of Sciences of the United States of America*, 2012, **109**, 12621-12625.
35. Y. Z. Tang, C. A. Zeiner, C. M. Santelli and C. M. Hansel, *Environ. Microbiol.*, 2012, In press.
36. D. R. Learman, B. M. Voelker, A. I. Vazquez-Rodriguez and C. M. Hansel, *Nature Geoscience*, 2011, **4**, 95-98.
37. C. M. Hansel and C. A. Francis, *Appl. Environ. Microbiol.*, 2006, **72**, 3543-3549.
38. W. E. Krumbein and H. J. Altmann, *Helgolander Wissenschaftliche Meeresuntersuchungen*, 1973, **25**, 347-356.
39. S. M. Webb, *Phys. Scr.*, 2005, **T115**, 1011-1014.
40. B. Ravel and M. Newville, *Journal of Synchrotron Radiation*, 2005, **12**, 537-541.
41. T. Ressler, S. L. Brock, J. Wong and S. L. Suib, *J. Phys. Chem. B*, 1999, **103**, 6407-6420.
42. B. Lanson, V. A. Drits, Q. Feng and A. Manceau, *Am. Mineral.*, 2002, **87**, 1662-1671.
43. E. Silvester, A. Manceau and V. A. Drits, *Am. Mineral.*, 1997, **82**, 962-978.
44. A. T. Stone and J. J. Morgan, *Environ. Sci. Technol.*, 1984, **18**, 450-456.
45. A. T. Stone and J. J. Morgan, *Environ. Sci. Technol.*, 1984, **18**, 617-624.
46. Y. Wang and A. T. Stone, *Geochim. Cosmochim. Acta*, 2006, **70**, 4477-4490.
47. W. G. Sunda and D. J. Kieber, *Nature*, 1994, **367**, 62-64.
48. Y. Ono, T. Matsumura and S. Fukuzumi, *Journal of the Chemical Society-Perkin Transactions 2*, 1977, DOI: 10.1039/p29770001421, 1421-1424.
49. W. G. Sunda and S. A. Huntsman, *Deep-Sea Research Part a-Oceanographic Research Papers*, 1988, **35**, 1297-1317.
50. J. J. Morgan, in *Metal Ions in Biological Systems, Vol 37: Manganese and Its Role in Biological Processes*, eds. A. Sigel and H. Sigel, 2000, vol. 37, pp. 1-34.
51. J. J. Morgan, *Geochim. Cosmochim. Acta*, 2005, **69**, 35-48.
52. R. W. Coughlin and I. Matsui, *J. Catal.*, 1976, **41**, 108-123.
53. D. L. Parkhurst and C. A. J. Appelo, *User's guide to PHREEQC (Version 2) - A computer program for speciation, batch-reaction, one-dimensional transport, and inverse geochemical calculations*, U. S. Geol. Surv. Water Res. Inv. Rept. 99-4259, 1999.

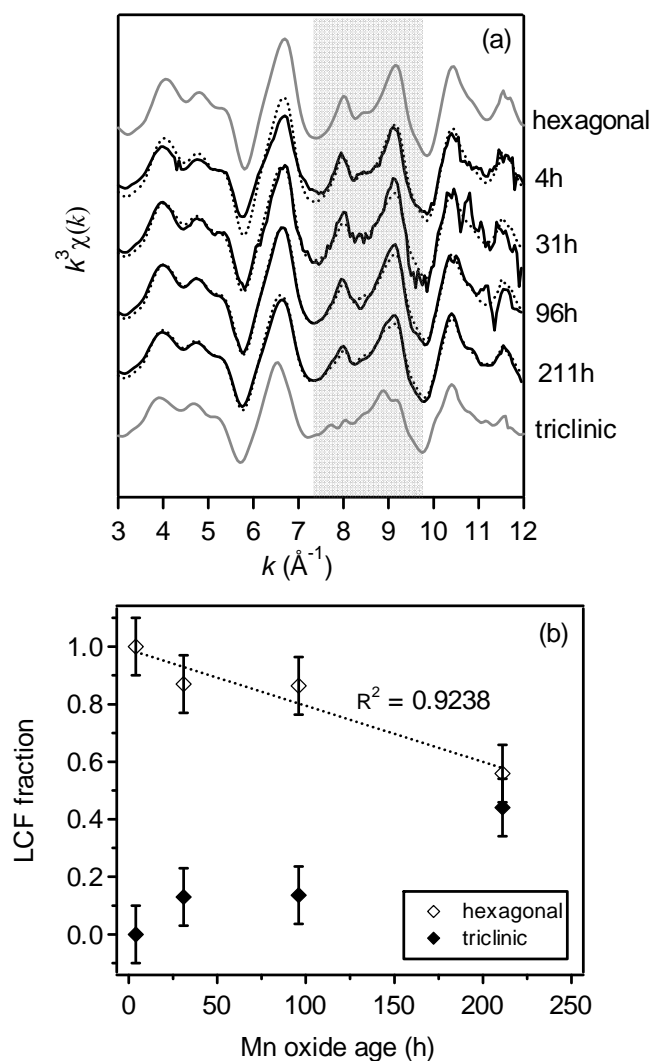


Figure 1. (a) Linear combination fitting (LCF) results of unreacted bioMnOx at different ages, with raw and fitted data in solid and dotted black lines, respectively. Also shown are the two end member spectra (gray lines) used for LCF, a hexagonal birnessite (δ -MnO₂) and triclinic Na-birnessite. (b) Corresponding LCF fraction of hexagonal and triclinic birnessite for the bioMnOx. Dotted line is a linear fitting of the hexagonal data ($R^2 = 0.9238$).

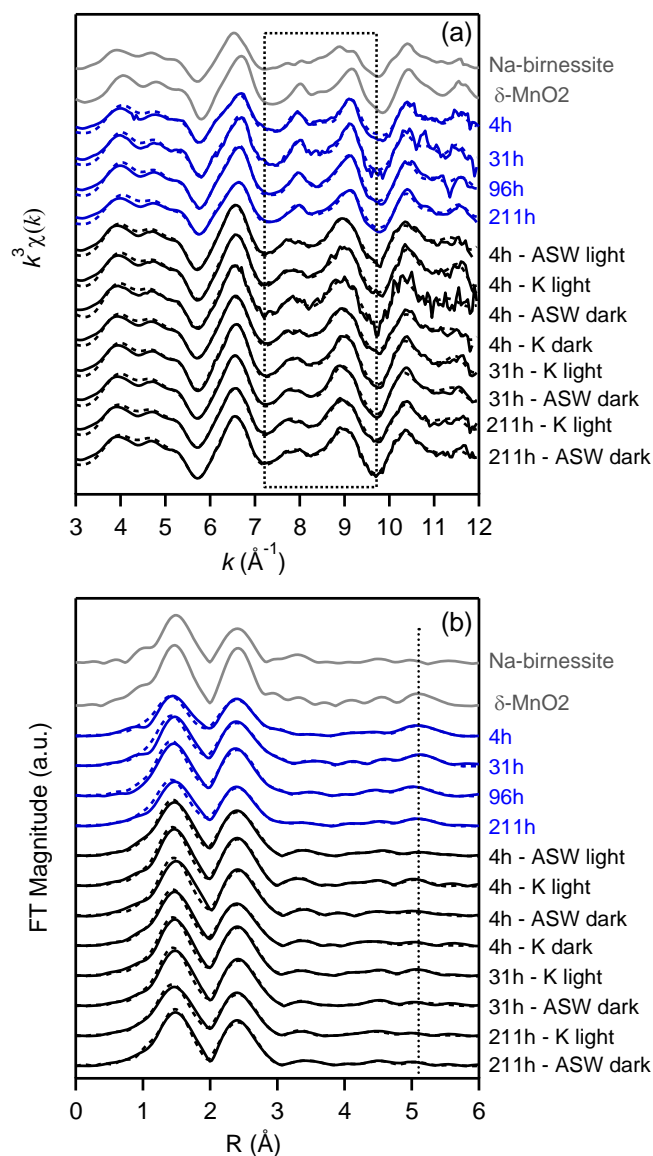


Figure 2. (a) Mn K-edge EXAFS data and (b) corresponding Fourier transforms of reference compounds (grey lines) and bioMnOx before (blue lines) or after (black lines) reacting with Cr(III) (~200 h). Raw and fitted data are shown in solid and dashed lines, respectively. Square with dotted line in (a) shows the “indicator” region of Mn EXAFS. Vertical dotted line in (b) labels the peak with major contributions from multiple scattering.

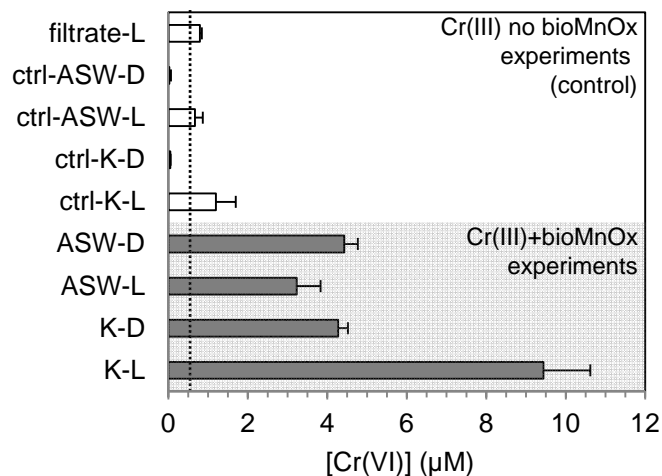


Figure 3. Amount of Cr(VI) produced in the presence of 4 h aged bioMnOx (filled bars) in artificial sea water (ASW) or K medium (K) at pH 7.2 under light (L) or dark (D) conditions. Also shown are the Cr(VI) production in control experiments (open bars), with the same amount of initial Cr(III) and no bioMnOx addition. They are conducted either in the cell-free filtrate, ASW, or K medium under light or dark conditions. Vertical dotted line is the averaged Cr(VI) production from all control experiments ($0.55 \mu\text{M}$). All values were measured when reactions reached near steady state (~ 200 h).

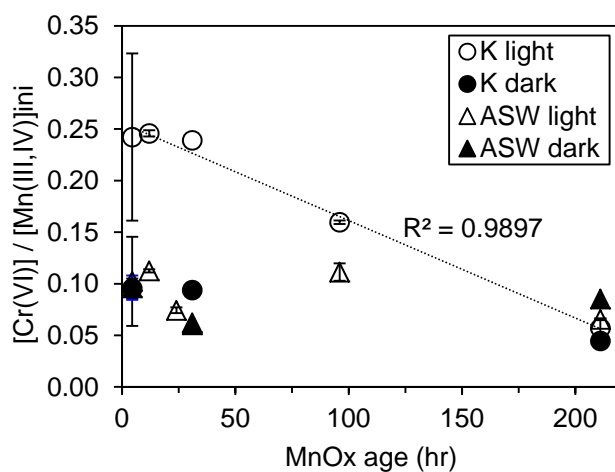


Figure 4. Cr oxidation capacity as a function of bioMnOx age when reacted in K medium or ASW under light or dark conditions. Dotted line is a linear fitting of the K light data ($R^2 = 0.9897$). Reactions were conducted at pH 7.2.

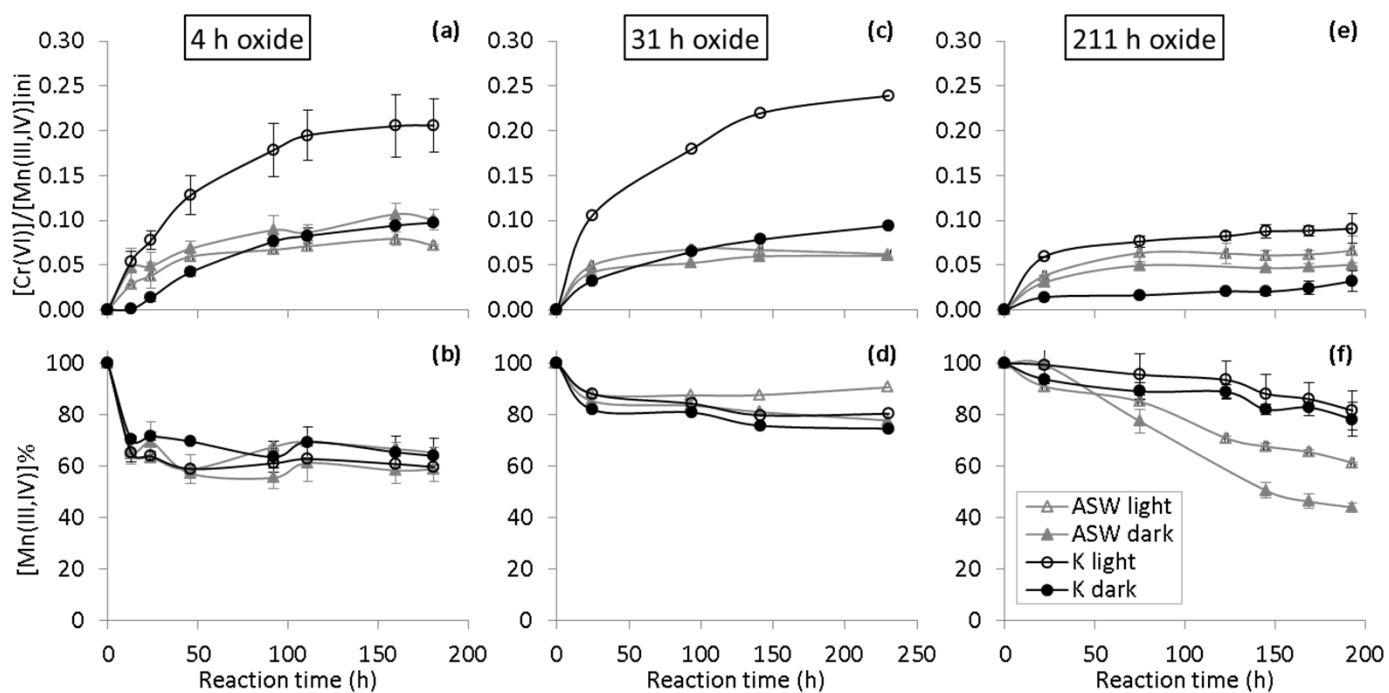


Figure 5. (a, c, e) Cr(III) oxidation capacity and (b, d, f) percent change of Mn(III, IV) oxide concentration as a function of reaction time in the K medium or ASW under light or dark conditions. BioMnOx ages are 4 h (a and b), 31 h (d and e), and 211 h (e and f)

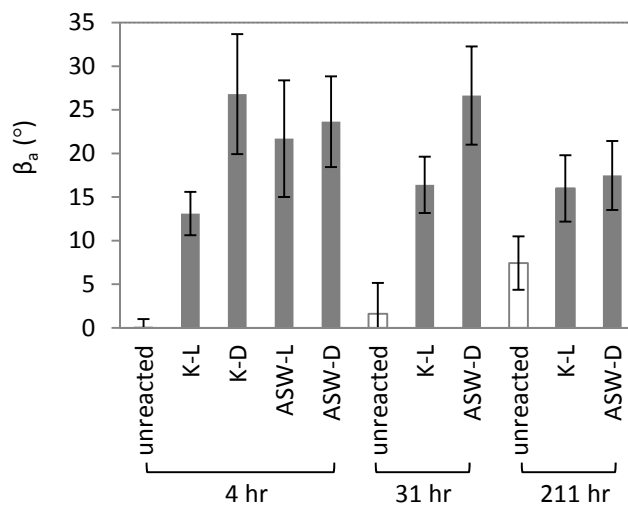


Figure 6. Comparison of the out-of-plane bending along a -axis (β_a angle) derived from EXAFS fitting of bioMnOx with different age and structural ripening before and after reaction with Cr(III) under different conditions.

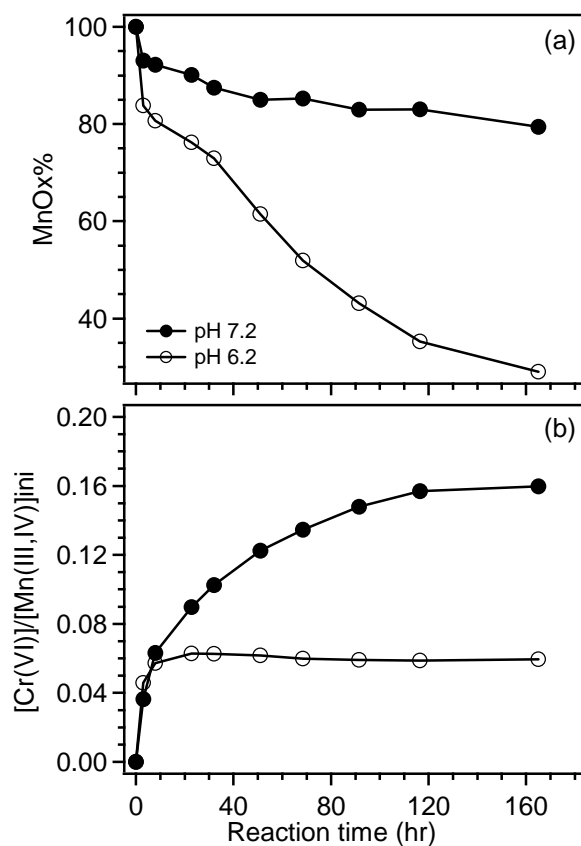


Figure 7. (a) Percent change of Mn(III,IV) oxide concentration and (b) Cr(III) oxidation capacity as a function of reaction time at pH 6.2 and 7.2. Reaction condition: 96 h aged bioMnOx, K medium, light condition.

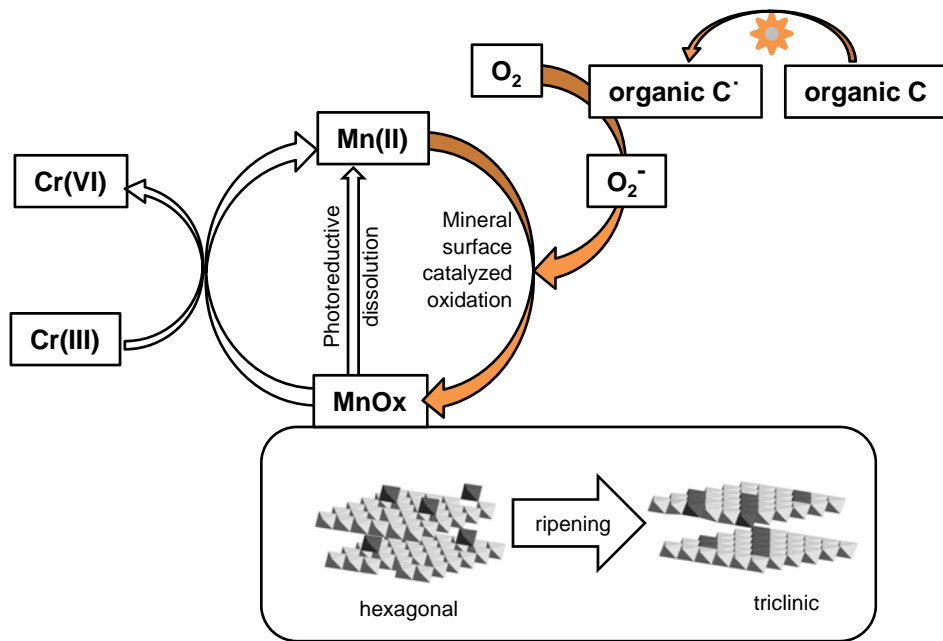


Figure 8. Schematic of possible reaction mechanism. Orange arrows represent reactions that occur only in the combined presence of organics and light.